Orbital Element Evolution due to Planetary Conjunctions: An Analysis Using Numerical and Analytical Techniques

Lizzy Jones
Advisor: Daniel Tamayo

28 April 2024

1 Introduction

The N-body problem is famously difficult to solve, as the gravitational interactions between planets alter their orbits as they travel. Understanding this complex system would not only illuminate a question which scientists have attempted to tackle for centuries, but it also has practical applications for satellite technologies. In this project, we look at a simplified version of a 3-body problem, specifically focusing on the interaction between two planets when one overtakes another as they orbit a larger star. In the limit that the planets' masses are small, this interplanetary interaction causes slight changes, or 'kicks' to the planets' orbital parameters at each planetary conjunction.

The effective potential for this interaction has been derived in explicit form by Namouni et al. using Fourier and Taylor series expansions [1]. In this project, we use Namouni's result to derive an analytical expression that describes the evolution in each planet's semi-major axis after a planetary conjunction. We also develop a computational simulation uses numerical integration to derive a solution for the same problem. Finally, we compare the two methods and demonstrate that they are consistent with one another.

2 Background

The generalized 3-body problem involves three massive bodies, each of which have three degrees of freedom. To simplify this setup, we study the case of the planar circular three body problem (PC3BP) with two planets orbiting a star in a plane. To further simplify the problem we consider the Hill Approximation, which is the limit in which the planets' masses m_1 and m_2 are small compared to the star, and the planets travel on closely-spaced, nearly-circular orbits [2]. Though this assumption may seem prohibitively restrictive, it is actually a reasonable approximation for many real-world systems (for instance, the Earth's eccentricity is only about 0.0034 and the Earth to Sun mass ratio is 3×10^{-6}) [3].

For the majority of the planets' orbits, the mechanics are dominated by the Sun's potential and any interplanetary interaction can be ignored. The interaction between planets

is only significant in the limit that the planets are very close to each other. The scale on which this interplanetary interaction is significant is called the Hill radius, R_H [1]. When the planets are one Hill radius apart, the gravitational pull between the two planets is exactly equal to the Sun's gravitational force that acts to tear them apart. The Hill Radius is defined by $R_H = a_0\epsilon$ where a_0 is the average semi-major axis of the two planets and ϵ is the small parameter defined as follows [1]:

$$\epsilon = \left(\frac{m_1 + m_2}{3M_\odot}\right)^{1/3}. \tag{1}$$

For the majority of the orbit during which the planets are further than one Hill radius apart, the three body problem reduces to two separate two body problems between the Sun and each planet. The challenge is to determine planetary motion around 'conjunction,' when the planets are at their closest as the inner planet overtakes the outer planet.

Our goal is to characterize the gravitational potential near conjunction and determine its effects on the orbital elements, namely the semi-major axis, a. Namouni et al. derive an expression for the effective potential of the system near conjunction for the three-dimensional case using a Fourier series expansion [1]. This expression is re-derived more briefly for the simple planar case in the following section, but we refer the reader to the Namouni paper for a more detailed, general analysis. Namouni et al. show that this potential can be used to derive a mapping between pre-conjunction and post-conjunction values of eccentricity e and semi-major axis a [1]. Using this mapping, we derive an analytical expression for the "kick" to a that occurs during conjunction in Section 3.4.

3 Analytical Solution

3.1 System Setup

Following steps taken by Namouni et al, we analyze the system in Hill's reference frame, which rotates at an angular velocity equal to the mean motion of the barycenter of the planets, $n = (G(M_\odot + m_1 + m_2)/a_0^3)^{1/2}$. The origin of the reference frame traces a circle of radius a_0 about the star, where a_0 is the semi-major axis of the barycenter's orbit.

It is helpful to define a set of relative coordinates in order to analyze the system. To determine the location of the planets, we use λ, which measures the relative angle between the position of both planets. Similarly, we use ϖ to measure the relative angle between the semi-major axes of the planetary orbits. We also define a as the difference in semi-major axes of the planets, $a_1 - a_2$. Finally, we define relative eccentricity e as follows:

$$\vec{e} = (e\cos\varpi, e\sin\varpi) = (h, k) = \vec{e_1} - \vec{e_2} \tag{2}$$

We non-dimensionalize all units, where time is normalized to $1/n$ and distance is normalized to $R_H = a_0\epsilon$. Using these variables, we can define a canonical set of variables for the system

as follows:

$$h = e\cos\varpi, \qquad k = e\sin\varpi, \tag{3}$$

$$Y = -3a(t-\lambda)/4, \qquad a. \tag{4}$$

Finally, we must define a function to describe the interplanetary gravitational potential. In our non-dimensionalized units, this potential can be expressed as $V(r) = -3/r$, where r is the distance between masses.

V is a function of distance r, which can equivalently be expressed in terms of the non-dimensionalized mean anomaly $M = t - \lambda$ and Y from Equation 4 as follows:

$$r^2 = x^2 + y^2 \tag{5}$$

$$x = e\cos M + 1 \tag{6}$$

$$y = -2e\sin M + 2Y \tag{7}$$

3.2 Expansion of the Potential

Recall that the potential function $V(M, Y)$ is only applicable in the limit that the planets are close (ie within one Hill radius of each other). Thus, if we integrate this potential over one entire cycle, we obtain the total increment in orbital elements due to the "kick" at conjunction. The total effective potential W of the cycle is then

$$W = \int_{-\infty}^{+\infty} V(M, Y)dt. \tag{8}$$

As Namouni et al. show, $V(M, Y)$ can be expanded as a Fourier series in M and subsequently a Fourier transform in Y. The effective potential becomes

$$W = \int_{-\infty}^{+\infty} dt \int_{-\infty}^{+\infty} d\omega \sum_{n=-\infty}^{+\infty} \tilde{V}(n, \omega)e^{j(\omega Y + nM)} \tag{9}$$

where $\tilde{V}(n, \omega)$ is the Fourier transform of $V(M, Y)$ in the variables n and ω. After integrating this expression over t and ω, Namouni et al. show that Equation 9 reduces to the following:

$$W = \frac{8\pi}{3} \sum_{n=-\infty}^{\infty} \tilde{V}(n, \frac{4n}{3})e^{in(\lambda-\varpi)} \tag{10}$$

$$= \sum_{q=-\infty}^{\infty} W_q e^{in(\lambda-\varpi)} \tag{11}$$

The coefficient W_q can be found by solving for $\tilde{V}(n,\omega)$ using Fourier analysis as follows. The Fourier transform derived in Equation 9 is performed successively in $M \to n$ then $Y \to \omega$. To find the appropriate Fourier coefficients, Namouni et al work from the inner function, first finding an expression for $\tilde{V}(\omega)$. Then, this result is used to find $\tilde{V}(n,\omega)$.

To find $\tilde{V}(\omega)$ recall that $V(r) = -\frac{3}{r}$. The Fourier transform in Y is:

$$\tilde{V}(\omega) = -\frac{1}{2\pi}\int_{-\infty}^{\infty} -\frac{3}{r}e^{-i\omega Y} \tag{12}$$

$$= -\frac{3}{2a\pi}K_0\left(\frac{\omega A}{2}\right)e^{iB\omega/2} \tag{13}$$

where $B = \frac{y}{a} - 2Y$ and K_0 is a Bessel function of the second kind. This result can then be Fourier analyzed in M to obtain the full expression $\tilde{V}(n,\omega)$:

$$\tilde{V}(n,4n/3) = \frac{1}{2\pi}\int_{-\pi}^{+\pi}\tilde{V}(4n/3)e^{-inM}dM \tag{14}$$

$$= -\frac{3}{4\pi^2 a}\int_{-\pi}^{+\pi}K_0\left(\frac{2n}{3}(e_*\cos M + 1)\right)dM \tag{15}$$

where $e_* = \frac{e}{a}$. Using this result along with the relationship between Equations 10 and 11, the full expression for the coefficient W_q becomes:

$$W_q = \frac{8\pi}{3}\tilde{V}(n,4n/3) \tag{16}$$

$$= -\frac{2}{a\pi}\int_{-\pi}^{+\pi}e^{-in(M+\frac{4}{3}e_*\sin M)}K_0\left(\frac{2n}{3}(e_*\cos M + 1)\right)dM \tag{17}$$

Taking a Taylor expansion around $e_* = 0$, we recover an expression for W_q as an expansion in powers of eccentricity e_*:

$$W_q = \frac{1}{a}\sum_{q=0}^{\infty}W_q^{q,0}e_*^q \tag{18}$$

This expression is derived in Namouni et al. for the more general three-dimensional case. The 0 term in the superscript of the $W_q^{q,0}$ is associated with the orbital inclination, but we can set this to zero since we are studying the planar case. These coefficients $W_q^{q,0}$ are evaluated numerically by Namouni et al using equation 17. To third order in q, the relative quantities are as follows:

$$W_1^{1,0} \approx 3.359350011 \tag{19}$$

$$W_2^{2,0} \approx -2.678665722 \tag{20}$$

$$W_3^{3,0} \approx 2.639498803 \tag{21}$$

3.3 Mathematical Mapping for Orbital Elements

Now that we have an explicit expression for the effective potential W, it is possible to determine how the planets' orbital parameters evolve throughout a conjunction. In particular, we seek the change in relative semi-major axis a during conjunction.

To obtain a mathematical mapping between pre-conjunction and post-conjunction values, it is useful to define the following action-angle variable pairs to characterize the orbital elements:

$$(\varpi, I) \quad \text{where } I = \frac{1}{2}\left(\frac{e}{\epsilon}\right)^2 \tag{22}$$

$$(\lambda, K) \quad \text{where } K = \frac{3}{8}\left(\frac{a_r}{a_0\epsilon}\right)^2 \tag{23}$$

We can express the effective potential W to second order in terms of these action-angle variables and the coefficients $W_q^{q,0}$ in Equations 19-21:

$$W = 2W_1^{1,0}\frac{\sqrt{2I}}{a^2}\cos\left(\lambda - \varpi\right) + \left(W_0^{2,0} + 2W_2^{2,0}\cos\left(2(\lambda - \varpi)\right)\right) \tag{24}$$

Note that the numerical coefficient $W_0^{2,0}$ arises from scenarios with nonzero inclination in the 3-dimensional case that Namouni considers. This does not apply to our planar problem, but because we will be taking the derivative of this function with respect to ϖ and λ in the next step, it does not affect the result.

Recall that the potential described in Equation 24 is only relevant within one Hill radius of the conjunction because we are using the Hill approximation in which the planets' masses are small. Thus we can treat the cumulative effect of this potential around one orbit as a discrete 'kick' at conjunction. As derived by Namouni et al, we can describe the change in orbital elements from conjunction n to conjunction $n+1$ using the following second-order mapping:

$$I_{n+1} = I_n + \frac{\partial W}{\partial \phi} \tag{25}$$

$$K_{n+1} = K_n - \frac{\partial W}{\partial \lambda}. \tag{26}$$

Taking the appropriate derivatives of W from Equation 24, the mapping is:

$$I_{n+1} = I_n - 2W_1^{1,0}\frac{\sqrt{2I_{n+1}}}{a^2}\sin\left(\lambda_n - \varpi_n\right) - 4W_2^{2,0}\sin\left(2(\lambda_n - \varpi_n)\right)\frac{2I_{n+1}}{a^3} \tag{27}$$

$$K_{n+1} = I_{n+1} - I_n + K_n. \tag{28}$$

Note again that all results up to this point are sourced directly from Namouni et al, which includes a more detailed derivation as well as more sophisticated mappings for more generalized cases [1].

3.4 Kicks to a at Conjunction

Using the mapping for orbital elements as derived above by Namouni et al, our goal is to determine the 'kicks' to the relative semi-major axis orbital element, a. Because we only need to consider a single conjunction for this purpose, we define $\Delta I = I_{n+1} - I_n$ and $\Delta K = K_{n+1} - K_n$ and drop the n notation elsewhere.

Equation 28 implies $\Delta K = \Delta I$. We can simplify this expression by substituting values $\sqrt{2I} = e/\epsilon$, crossing eccentricity $e_c = a/a_0$, and $\tilde{e} = e/e_c$. Note that the value of relative semi-major axis a must be negative in the mapping equations (see Equation 27), since $a = (a_1 - a_2)/(a_0\epsilon)$ where a_1 corresponds to the inner planet and a_2 corresponds to the outer planet. Therefore, all odd powers of a are negative. Furthermore, note that the $W_q^{q,0}$ values accompanying terms with odd powers of a are always negative, while those accompanying terms with even powers of a are always positive. In both cases, then, we can just take the absolute value of both a and $W_q^{q,0}$. The expression reduces to the following:

$$\Delta K = -2|W_1^{1,0}|\frac{\epsilon}{e_c}\tilde{e}\sin(\lambda - \varpi) - 4|W_2^{2,0}|\frac{\epsilon}{e_c}\tilde{e}^2\sin(2(\lambda - \varpi)) \tag{29}$$

Finally, we can use ΔK to determine the change in relative semi-major axis, a. Recall that K and a are related through the following expression as defined in Equation 23:

$$K = \frac{3}{8}\left(\frac{a}{a_0\epsilon}\right)^2. \tag{30}$$

Taking the derivative of Equation 30, we obtain a relationship between ΔK and the 'kick' to a, Δa:

$$\Delta K = \frac{3}{4}\frac{a}{(a_0\epsilon)^2}\Delta a. \tag{31}$$

Equating this value of ΔK to the first-order approximation in Equation 29 and substituting $\epsilon^3 = \mu/3$ yields a first order approximation for the kicks in a at conjunction:

$$\frac{\Delta a}{a_0} = -\frac{8}{9}\frac{\tilde{e}\mu}{e_c^2}\sin(\lambda - \varpi). \tag{32}$$

Performing a similar analysis on the second and third order terms, we can extrapolate the full expression as an expansion in order q as follows:

$$\frac{\Delta a_r}{a_0} = -\frac{8}{9}\frac{\mu}{e_c^2}\sum_{q=1}^{\infty} q\tilde{e}^q \sin\left(q(\lambda - \varpi)\right)|W_q^{q,0}|. \tag{33}$$

4 Computational Solution

4.1 Setup

To compare and verify our analytically-derived result, we developed a numerical N-body simulation in Python using REBOUND. REBOUND is an open-source Python package which enables us to set up a configuration of planets with specified orbital elements. Then, we use builtin integration methods to numerically integrate the system in time over a conjunction event. By tracking the positions of each object throughout this process, we can determine a numerical value for $\frac{\Delta a}{a_0}$, which can be compared the analytical solution derived in Equation 33.

To simplify the system, instead of studying the generalized planar three body system we consider a massless outer 'test particle' planet and a massive inner planet. This allows us to study the behavior of a third body– the massless test particle– without it influencing the rest of the system. The massive planet travels in a circular orbit of radius a_0, while the test particle has a slightly eccentric orbit. We initialize the simulation with the initial conditions described in Table 1.

Table 1: Initial Conditions for REBOUND Numerical Simulation

Parameter	Value
$\mu = m_1/M_\odot$	3.75×10^{-10}
ϖ_2 (test particle pericenter)	$\pi/2$ rad
n_1 (mean motion)	2π rad
$\tilde{e}$	0.1
λ_1	5.959 rad
λ_2	4.733 rad

The system configuration is plotted in Figure 1, where Figure 1a illustrates the initial positions of the planets and Figure 1b illustrates their positions after integrating in time to conjunction. In Figure 1, the system is initialized as a 7:6 mean motion resonance (MMR). This means that if the planet and test particle begin at the same angle λ, the inner planet must orbit 7 times and the outer test particle orbits 6 times before a second conjunction occurs. The 7:6 resonance is used strictly for illustrative purposes. For the remainder of the report, we initialize the system at a 100:99 MMR, which ensures the planet and test particle are closely-spaced. Note also that the mass of the planet and the eccentricity of the test particle are both small (see Table 1). These conditions ensure the Hill approximation is valid.

4.2 Numerical Integration

To perform integration, we use REBOUND's built-in symplectic second-order integrator. Symplectic integrators are a commonly-used algorithm for solving Hamilton's equations, especially in branches of physics that study Hamiltonian systems like celestial mechanics [4].

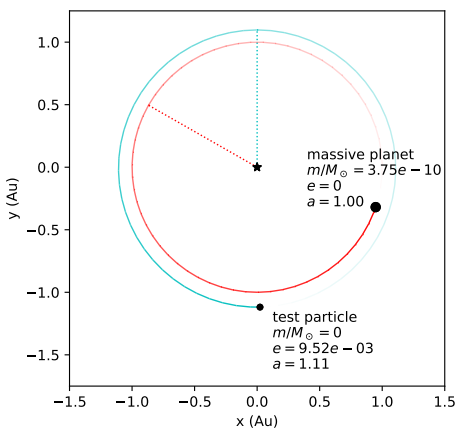

(a) Initial setup of the system. Values for relative mass $\mu = m/M_\odot$, eccentricity e, and semi-major axis a are indicated on the Figure for each object. Note that the semi-major axis of the massive planet is normalized to 1.

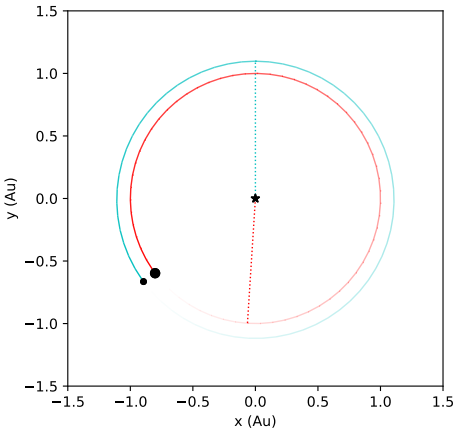

(b) Configuration of the system after integrating to conjunction. Note that the massive inner planet and outer test particle are located at the same angle, as is expected at conjunction.

Figure 1: Position plots of the planet and test particle

According to Liouiville's theorem, the volume of a Hamiltonian's phase space is conserved as the system evolves through time. This entails that the flow of the Hamiltonian (ie the mapping that steps the solution forward in time) is a symplectic transformation [4]. Symplecticity places additional constraints on the problem, as the solutions of Hamilton's equation must exist inside the symplectic manifold.

A symplectic integrator is a numerical technique which ensures the solution lies on the symplectic manifold. There are several types of symplectic integration methods, including the symplectic Euler scheme, the Störmer-Verlet scheme, and the symplectic Runge-Kutta scheme [4]. Such methods are described in more detail in Chapter VI of Symplectic Integration of Hamiltonian Systems by Lubich, Ernst, and Wanner [4]. Due to discretization error symplectic integrators often diverge from the true solution space over long integration times. However, because they constrain the possible solution space much more strongly than traditional non-symplectic integrators, they are far more accurate [5]. While symplectic integrators experience linear drift over time, non-symplectic integrators undergo quadratic or even higher order drift [5].

4.3 Results

Using the second order symplectic integrator, we integrated our system over a conjunction event. A plot of the relative semi-major axis a vs time for this process is shown Figure 2. The value of a prior to conjunction, a_i is annotated as an orange horizontal line. As time passes

and the planets near the conjunction event, they become closer until they are eventually less than one Hill radius apart. At this point, the interplanetary interaction attracts the test particle to the planet, decreasing the relative semi-major axis $a = a_2 - a_1$ (note that we have redefined a to be positive in keeping with the conventions described in the previous section). This decrease is visible in the plot at $t = 0$, where the sharp downward spike signifies the conjunction event. As the planets separate again, they settle at the post-conjunction value a_f, which is annotated as a green horizontal line. As described by the Hill approximation, the planetary conjunction can be approximated as a discrete event to a high degree of accuracy, and the relative semi-major axis a is nearly constant between conjunctions. This verifies that the Hill approximation holds for our chosen initial conditions. The values of a_i and a_f can thus be used to find a numerical value for $\frac{\Delta a}{a_0}$.

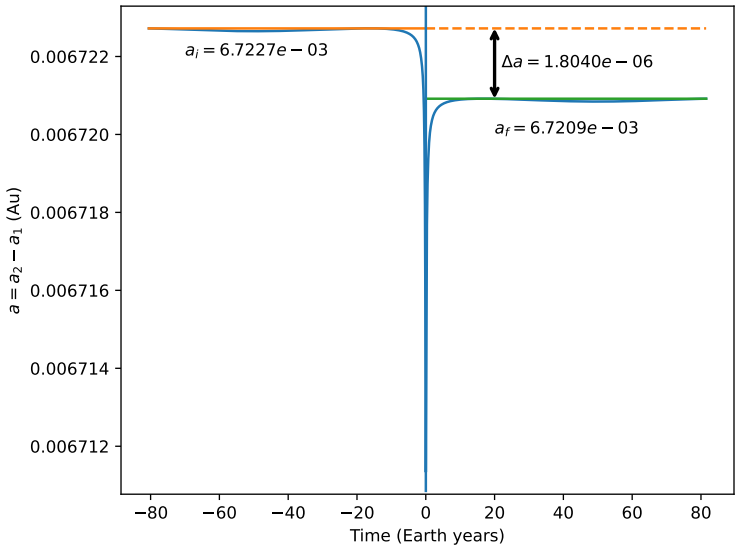

Figure 2: Relative semi-major axis between the massive inner planet and massless outer test particle plotted as a function of time throughout a conjunction event, which occurs at $t = 0$. Pre-conjunction and post-conjunction values of a are included in the orange and green horizontal lines, respectively. Note that the units are normalized so that $a_0 = 1$.

To compare the numerical model to the analytical result, we run the simulation for a range of 10 different $\tilde{e}$ values evenly spaced from 0.001 to .1. For each value of $\tilde{e}$, we integrate for a total of 100000 time steps and record the values of a throughout this process to determine a_0 and a_f. These values can be used to determine the kicks in relative semi-major axis as follows:

$$\frac{\Delta a}{a_0} = \frac{a_f - a_i}{a_0}. \tag{34}$$

We can then match our numerical values of $\frac{\Delta a}{a_0}$ to the analytical result derived using Equa-

tion 33 and the given values for μ, $\tilde{e}$, and Namouni's calculations for $W_q^{q,0}$. Our results for the computational and analytical solutions are plotted against each other in Figure 3.

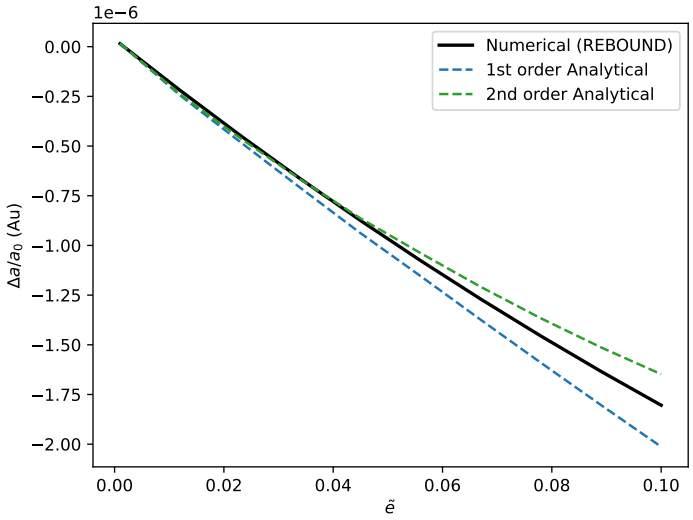

Figure 3: Comparison of analytical and numerical solutions for kicks to relative semi-major axis after a planetary conjunction. The first order approximation for the analytical solution is plotted in blue, and the second order approximation is plotted in green. The two solutions are in close agreement.

As this figure illustrates, our analytical and numerical results are in close agreement. In particular, note that the second order term of the analytical solution significantly improves the first order approximation, as expected. This correlation confirms the accuracy of our derived expression for the kicks in a (Equation 33). The two solutions diverge beginning around $\tilde{e} = 0.05$, even when higher order terms of the analytical solution are included. This is because the analytical expression was derived as an expansion about $e_* = 0$ where $e_* = \frac{e}{a}$ and is thus only valid for small values of $\tilde{e}$.

5 Conclusion and Future Work

Studying the simplified PC3BP, we analyze the change in a planet's orbital parameters (namely the relative semi-major axis a) due to a planetary conjunction. Our analysis includes two techniques– numerical integration as well as analytical analysis using Fourier expansion– and demonstrates that these methods are consistent with one another. Our next task is to verify this result for higher order resonances (ie a second order 100:98 MMR instead of the first order 100:99 MMR). The coupling strength in resonant MMRs is known to behave as e^k where k is the order of the resonance, so our ultimate goal is to verify this result numerically by building upon the REBOUND simulation from this project.

References

[1] F. Namouni et al. "A mapping approach to Hill's distant encounters: application to the stability of planetary embryos." In: *Astronomy and Astrophysics* 313.3 (1996), pp. 979–992.

[2] M. Henon and J. -M. Petit. "Series Expansions for Encounter-Type Solutions of Hill's Problem". In: *Celestial Mechanics* 38.1 (Jan. 1986), pp. 67–100. DOI: 10.1007/BF01234287.

[3] Dave Williams. *Sun fact sheet*. URL: https://nssdc.gsfc.nasa.gov/planetary/factsheet/sunfact.html.

[4] Ernst Hairer, Christian Lubich, and Gerhard Wanner. *Geometric numerical integration. Structure-preserving algorithms for ordinary differential equations. 2nd ed.* Vol. 31. Jan. 2006. ISBN: 3-540-30663-3. DOI: 10.1007/3-540-30666-8.

[5] Chris Rackauckas. *Stochastic lifestyle*. URL: http://www.stochasticlifestyle.com/.